2017-08-16

Aeolian sediment fingerprinting using a Bayesian mixing model

Gholami, H

10.1002/esp.4189
Earth Surface Processes and Landforms
Wiley

Earth Surface Processes and Landforms

Aeolian sediment fingerprinting using a Bayesian mixing model

Journal:	*Earth Surface Processes and Landforms*
Manuscript ID	ESP-17-0002.R1
Wiley - Manuscript type:	Research Article
Date Submitted by the Author:	n/a
Complete List of Authors:	Gholami, Hamid; University of Hormozgan, Department of Range and Watershed Management Telfer, Matt; Plymouth University, School of Geography, Earth and Environmental Sciences Blake, William; Plymouth University, SoGEES Fathabadi, Abolhassan; University of Gonbad-e-Kavoos, Department of Range and Watershed Management
Keywords:	Aeolian sediment, Sand provenance, Markov Chain Monte Carlo, Fingerprinting, Dune

Aeolian sediment fingerprinting using a Bayesian mixing model

Hamid Gholami [a*], Matt W. Telfer [b*], William H. Blake [b] and Abolhassan Fathabadi [c]

[a] Department of Range and Watershed Management, University of Hormozgan, Bandar-Abbas, Hormozgan, Iran.

[b] School of Geography, Earth and Environmental Sciences, Plymouth University, Plymouth, Devon, PL4 8AA , UK.

[c] Department of Range and Watershed Management, University of Gonbad-e-Kavoos, Gonbad-e-Kavoos, Golestan, Iran.

* Correspondence to:

Hamid Gholami, Department of Range and Watershed Management, University of Hormozgan, Bandar-Abbas, Hormozgan, Iran. *E-mail address*: hgholami@hormozgan.ac.ir. Tel: +98 937 0865077.

and

Matt Telfer, School of Geography, Earth and Environmental Science, Plymouth University, Plymouth, Devon, PL4 8AA, UK. *E-mail address*: matt.telfer@plymouth.ac.uk. Tel: +44 1752 585570.

Abstract

Identifying sand provenance in depositional aeolian environments (e.g. dunefields) can elucidate sediment pathways and fluxes, and inform potential land management strategies where windblown sand and dust is a hazard to health and infrastructure.

However, the complexity of these pathways typically makes this a challenging proposition, and uncertainties on the composition of mixed-source sediments are often not reported. This study demonstrates that a quantitative fingerprinting method within the Bayesian Markov Chain Monte Carlo (MCMC) framework offers great potential for exploring the provenance and uncertainties associated with aeolian sands.

Eight samples were taken from dunes of the small (~58 km^2) Ashkzar erg, central Iran, and forty-nine from three distinct potential sediment sources from the surrounding area. These were analyzed for 61 tracers including 53 geochemical elements (trace, major and rare earth elements (REE)) and 8 REE ratios. Kruskal–Wallis H-tests and stepwise discriminant function analysis (DFA) allowed the identification of an optimum composite fingerprint based on six tracers (Rb, Sr, ^{87}Sr, $(La/Yb)_n$, Ga and δCe), and a Bayesian mixing model was applied to derive the source apportionment estimates within an uncertainty framework.

There is substantial variation in the uncertainties in the fingerprinting results, with some samples yielding clear discrimination of components, and some with less clear fingerprints. Quaternary terraces and fans contribute the largest component to the dunes, but they are also the most extensive surrounding unit; clay flats and marls, however, contribute out of proportion to their small outcrop extent. The successful application of these methods to aeolian sediment deposits demonstrates their potential for providing quantitative estimates of aeolian sediment provenances in other mixed-source arid settings, and may prove especially beneficial where sediment is derived from multiple sources, or where other methods of provenance (e.g. detrital zircon U-Pb dating) are not possible due to mineralogical constraints.

Key words: Sand provenance; Aeolian sediment; Markov Chain Monte Carlo; Fingerprinting; uncertainty.

1. Introduction

Identifying and quantifying the source(s) of aeolian sediments is a long-standing challenge for geoscientists, and yet such information is often of crucial importance in understanding sediment fluxes at a range of scales. As well as providing fundamental knowledge on long-term landscape evolution (e.g. Pell et al., 1997), aeolian provenance studies have been used to elucidate past wind regimes and palaeoclimates (e.g. Nanson et al., 1995), investigate hazardous dust transport pathways (e.g. Pethierick et al., 2008; Yang et al., 2007) and inform studies of the palaeoclimatic record of the Antarctic ice-core dust record (Delmonte et al., 2010; Delmonte et al., 2004). The challenges with the task arise not just from the diverse range of potential sources for aeolian sands and dusts (e.g. geological or lithological units, soil units, land use types and geomorphological landscapes), and the long transport distances which may be involved (on the order of 10-10^2 km for aeolian sand and 10-10^3 km for aeolian dust), but also the potential complexity of transport pathways (Huntsman-Mapila et al., 2005). Before deposition at its current location, an aeolian sand grain may have been through multiple cycles of fluvial, aeolian, lacustrine and/or colluvial deposition and subsequent mobilization. Aeolian sands, therefore, rarely retain an easy-to-interpret signature of their origins.

The use of geochemical fingerprinting methods to determine sediment provenance has progressively increased since the late 1990s (Walling, 2013). Application has been focused most widely in fluvial contexts (Haddadchi et al 2013) wherein there recent work has highlighted the need to pay attention to challenges in signature development and tracer behavior (Koiter et al., 2013). Sediment fingerprinting involves the identification, quantification and statistical testing of a range of source

material properties capable of discriminating between potential sediment sources with a view to improving knowledge of sediment source and transport processes (Collins et al., 2017) . These properties may include geochemical characteristics (e.g. Douglas et al., 2009; Lin et al., 2015), radionuclide concentrations (Wilson et al., 2012), mineralogy (Pittam et al., 2009), geochronological data (principally U-Pb dating of detrital zircons; e.g. Pell et al., 1997; Garzanti et al., 2013), biomarkers (Chen et al., 2016) and colour properties (Martínez-carreras et al., 2010). Although sediment fingerprinting studies of aeolian sands are not new (e.g. Pell et al., 1997; Wasklewicz and Meek, 1995; Winspear and Pye, 1996; Liu et al., 2016; Muhs et al, 2017), challenges remain in adequately capturing the uncertainties associated with the diverse sources and pathways that may exist, and adoption of techniques developed in different disciplines offer a route forward. It is noteworthy that in a recent review discussing applications of sediment source-tracing methods (Owens et al., 2016), mention of aeolian sedimentation is limited to health science studies of PM2.5 and PM10 material. The opportunity to utilize these approaches in aeolian process science remains largely overlooked.

In recent years, increasing attention has been directed to the uncertainty of the results generated by sediment source fingerprinting. It is important that such uncertainty is recognized, particularly if the results are to be used to target investment in sediment control measures (Mukundan et al., 2012). The factors contributing to uncertainty in estimates of source apportionment are manifold and diverse, and have been reviewed elsewhere (e.g. Walling 2010; Koiter et al., 2013; Collins et al, 2017); here we consider some of the differences between the fluvial setting of most sediment fingerprinting studies, and the aeolian context considered

here. Many uncertainties remain the same – for instance, instrumental precision. Other aspects of the aeolian entrainment, transport and depositional system, however, differ markedly from fluvial settings. Due to dominance of gravity in controlling - and directing - slope and fluvial processes, and the (usually) confined nature of fluvial systems, erosion and entrainment of sediment from catchments is highly directionally-controlled. In an aeolian context, there is more scope for spatially extensive direct entrainment of sediment, and also more potential for directional variability, and this complex mixing environment may in turn lead to increased covariance between properties used to derive the fingerprint. In addition, such complexities cannot be considered static, as variations in wind regimes over long timescales may lead to changes in these pathways.

In order to quantify the uncertainty associated to mixing models related to this inherent variability in the source area and sediment mixture data, some recent studies have explored the use of Monte Carlo simulations (e.g. Motha et al., 2003; Collins et al., 2013; Collins et al., 2012; Stone et al., 2014; Smith & Blake, 2014; Sherriff et al., 2015; Vale et al., 2016; Gellis & Noe, 2013; Voli et al., 2013; Wilkinson et al., 2013; Walling et al., 2008). More recently, Bayesian mixing models being employed more comprehensively translate component uncertainties into source apportionment results (Cooper and Krueger, 2017) with several examples undertaken in hydrological contexts (e.g. Fox & Papanicolaou, 2008; Cooper et al.,2014; Cooper et al., 2015; Nosrati et al., 2014; Stewart et al., 2015). To date, however, such approaches have not been used within aeolian sedimentary contexts.

The sophistication of aeolian sediment provenance studies currently lags those in the fluvial sphere, and the main aim of this paper is to demonstrate the viability of fingerprinting methods for aeolian sediments, including the estimation of uncertainty, associated with the contributions from different geological units as potential sources for a small dunefield, Ashkzar Erg, in the Yazd-Ardekan Plain, central Iran, using a Bayesian mixing model. Ashkzar erg and its surrounding potential sources cause many serious problems related to wind erosion and associated on-site and off-site effects, with potential impacts on the health of the occupants of the neighbouring city of Yazd (Naddafi et al., 2006). Aeolian deflation is a major erosional process on the Yazd-Ardekan Plain and large amounts of aeolian sediment are often transported to residential regions by wind (Amiraslani and Dragovich, 2011). Therefore, quantifying sediment source contributions to the Ashkzar sand dunes could help to select the best management strategies at this location and others similarly affected by aeolian erosion. Additionally, the findings are considered in their geomorphological context with the aim of explaining the spatial variability in sediment provenance observed at Ashkzar erg.

2. Materials and methods

2.1. Field location

Yazd-Ardekan (31º10′–32º43′N, 53º68–54º47′E) is an arid plain in central Iran, and includes different geomorphic landscapes, such as the Ashkzar and Yazd ergs (Figure 1). The Yazd-Ardekan Plain is surrounded by mountain ranges. These are Shirkooh in the south, Ahangaran and the Margh Zard Mountains in the west, Haft Adamin and Khoonzad Mountains in the east and Chak Chak Mountain in the north. The area of the plain is ~2900 km^2, and it consists of 78% Quaternary alluvial fans

and terraces (Qt_2 geological unit), 13% clay flats (Qc geological unit), 7% Eocene gypsiferous marl (Egm geological unit) and 2% sand dunes (Qsd geological unit) (Figure 1 and 2). About 93% of Yazd-Ardekan Plain is thus covered by Quaternary deposits. Active and stabilized sand dunes in the Ashkzar erg occupy 58 km^2 (centred on 32° 1'N, 54° 10'E), which is dominated by barchans and transverse barchanoid ridges (Figure 2). The erg has a sparse but extensive cover of *Haloxylon persicum*, a species which is both endemic to the region, and is also used to stabilize mobile sand (Amiraslani and Dragovich, 2011). Based on 50 years of climate data at Yazd Meteorological Station, minimum and maximum annual temperatures are -16 °C and 46 °C, respectively. Long-term mean rainfall and annual evaporation in the study area are ~60 mm/year and ~3500 mm/year respectively. According to annual wind roses, dominant winds on the Yazd-Ardekan Plain are mainly from the north and west (Figure 1C).

[Approx. location of Figure 1]

2.2. Sampling and laboratory analysis

The geological units that were identified as potential sources for sand dunes (Qsd formation) are the Qt2 (Quaternary alluvial fans and terraces), Qc (Quaternary clay pans and flats) and Egm (Eocene marls) formations. Other surrounding lithologies in the vicinity are hard, igneous exposures and can be discounted from generating substantial quantities of deflatable sediment. In this study, spatially distributed source samples were taken from 49 sites, covering the Egm (n=8), Qc (n=18) and Qt2 (n=23) potential sources, and eight sediment samples were collected from the Ashkzar sand dunes (Figure 1D). Samples were collected from the upper 0–5 cm

depth of potential sources (that is, the layer of the regolith exposed to current aeolian entrainment) and sand dunes (that is, the layer of the regolith most recently deposited); this is similar to sampling strategies employed by other provenance studies of aeolian dunes (e.g. Pell et al., 1997), and is accordance with common earth science protocols (Owens et al., 2016). Within each source area, sample selection was based upon locations that were: a) clearly derived from the geological unit in question, b) selected to ensure broad spatial coverage of the source area, and c) clearly influenced by aeolian erosion (e.g. the presence of deflatable unvegetated sand surfaces with ripples, as well as yardangs of a range of scales). Samples numbers were chosen to ensure a balance between the greater spatial extent of the Qt2 unit (i.e. sampling was stratified), whilst maintaining a minimum of eight samples for the smaller Egm and Qc units. The spatial location of sampling sites is shown in Figure 1D.

All sand dune and potential source samples were dry sieved for particle size data, and to isolate the 62.5-150 μm fraction for further geochemical analysis. This fraction was chosen as it represents the dominant fraction in each of the dune samples (Table 1), and is of a size range susceptible to aeolian transport (whilst excluding any contribution of larger grains from local sources, either by aeolian creep or other transport processes). Concentrations of elements including major, trace and rare earth elements (REE) were determined using ICP-MS, after direct digestion with aqua regia (e.g. Collins et al., 2010; Collins et al., 2012); and concentration of strontium and neodymium isotopes measured by ICP-MS, after digestion with a mixture of HNO_3+$HClO_4$+HF (3:2:1) (e.g. Honda et al., 2004; Rao et al., 2011). The relative standard deviation (%RSD), based on three replicates for each determinant on each sample, was consistently ≤ 4%. With regards to REE concentrations, eight

REE ratios including ∑REE, Nd/Yb, Eu/Eu* (Europium Anomaly), $(La/Lu)_n$, $(La/Sm)_n$, $(Gd/Yb)_n$, $(La/Yb)_n$ and δCe (Cerium Anomaly) were calculated (e.g. Daga et al., 2008; Dou et al., 2010; Rao et al., 2011). In total, 61 tracers were used to fingerprint the sediments of the Yazd-Ardekan Plain.

[Approx. location of Table 1]

[Approx. location of Figure 2]

[Approx. location of Figure 3]

2.3. Discrimination of aeolian sediment sources

We employed a two-stage statistical method proposed by Collins and Walling (2007) to characterize the composite fingerprint for the sources of the sands of the Ashkzar dunes. In stage one, all individual fingerprint properties were tested for their ability to distinguish source types, using the Kruskal–Wallis H-test. Properties with critical values at the 95% level of confidence could be used in a composite fingerprinting model to discriminate between sources types. In stage two, stepwise discriminant function analysis (DFA) was employed to identify the optimum composite fingerprint model from the properties selected in stage one. The stepwise DFA was based on the minimization of Wilk's lambda was used to select optimum composite fingerprint. The F values were used as the test criteria to enter and remove elements. The threshold of F value for entering and removing of elements was set to 3.84 and 2.71, respectively (e.g. Vale et al, 2016).

2.4. Bayesian mixing model

End-member mixing models have been taken a variety of approaches to account for uncertainty in the mixing model (Cooper and Krueger, 2017) and some (e.g. Brewer et al., 2005; Fox & Papanicolaou, 2008) have adopted hierarchical Bayesian models, which we adopt here. Within the mixing model formulation, we assume that, for each source *s*, the sample i tracer composition, x, has a multivariate normal distribution as follows:

$$x_s^i \sim \mathrm{MVN_A}(\mu_s, \sum_s), \qquad s = 1, \ldots, N, \quad i = 1, \ldots, n_{x,s} \qquad \text{(eq. 1)}$$

where $n_{x,s}$ indicates the number of samples of source *s*; μ_S is a A-dimensional vector representing mean fingerprints for source s; $\sum_s$ represents a *(A × A)* dimensional covariance matrix for source s. There are n_z sediment samples for which *A* fingerprints were measured for each sample $Z^j = (z_1^j, \ldots, z_A^j)^T, j = 1, \ldots, n_z$ and these fingerprints have multivariate normal distributions:

$$Z^j \sim \mathrm{MVN_A}\left(\mu_j^z, \sum^z\right) \qquad \text{(eq. 2)}$$

Each source *s* has a fractional contribution p_s^j to each sediment sample *j*. The contribution of source types for each sediment sample is equal to $p_s^j y_s^j$, where y_s^j is an unobserved (latent) variable that follow the same distribution as X_s^i.

$$\mu_j^z = \sum_{s=1}^N p_s^j y_s^j \ , \qquad j = 1, \ldots, n_z \qquad \text{(eq. 3)}$$

$$\sum_{s=1}^N p_s^j = 1, \quad 0 \le p_s^j \le 1 \qquad \text{(eq. 4)}$$

Each fractional contribution must be between zero and one, positive and all of them must sum to unity. To meet this constraint, some studies have used Dirichlet distribution as a prior for the fractional contribution (e.g. Fox & Papanicolaou, 2008; Massoudiehet al., 2013), whereas other studies used transformation such as

centered log-ratio (CLR) (Semmenset al., 2009), isometric log-ratio (ILR) (e.g. Cooper et al., 2015; Parnell et al., 2013; Egozcue et al., 2003) and additive log-ratio (ALR) (e.g. Brewer et al., 2005; Palmer & Douglas, 2008). In this study, a CLR transformation was used, as it has been shown to produce comparable median values to other methods, but with better precision (Cooper et al., 2014). The transformation applied is thus:

$$\phi_i = CLR(P_i) = \log[\frac{P_{i1}}{g(P_i)}, \dots, \frac{P_{ik}}{g(P_i)}] \quad \text{(eq. 5)}$$

$$\phi_{i\sim}(\mu_\emptyset, \boldsymbol{\tau}_\emptyset) \quad \text{(eq. 6)}$$

where $g(p_i)$ is the geometric mean of the proportion vector. Figure 4 shows a directed acyclic graph of the model. Compared to an empirical Bayesian approach in which some prior parameters are estimated using deterministic data, the full Bayesian approach employed here needs to specify prior distribution for all parameters. When there is little information about the parameters, using informative hyper-parameters cause biased results. In this study, weakly or non-informative hyper-parameters were used. Multivariate normal and inverse-Wishart distributions were selected as prior distribution for sources means and covariance matrix, respectively.

$$\mu_s^X \sim MVN(\theta_s, \tau_s^{-1}), \quad s = 1, \dots, N \quad \text{(eq.7)}$$

$$\sum_s^X \sim Inverse - Wishart(\Omega_s^X, \rho_s^X), \quad s = 1, \dots, N \quad \text{(eq.8)}$$

Here, the hyper-parameter θ_s was set to the sample means of the fingerprints and τ_s was set as a diagonal matrix with values 0.01 on the diagonal. For Wishart distribution, the hyper-parameter Ω_s^X is a diagonal matrix with value 1 as diagonal

elements and ρ_S^X was set to six (to reflect the lack of information on the precision matrices, and the number of tracers selected for the fingerprint). Similar prior distribution and hyper-parameters was assigned for sediment covariance matrix.

$$\sum^Z \sim Inverse - Wishart(\Omega, \rho) \quad \text{(eq.9)}$$

Weakly informative hyper-parameters N(0,1) and Inv-Γ(2,1) were assigned for μ_ϕ and τ_ϕ, respectively.

The complete posterior distribution of all model parameters for sediment sample Z_j can thus be written as

$$\left(\Sigma_S, \tau_\phi, \mu_\phi, \Sigma^Z, p_j, \phi, \mu_S | X, Z_j\right) \propto \prod_{S=1}^{N} \prod_{i=1}^{n_{x,s}} \{P\left(x_s^i | \mu_S, \Sigma_S\right)\} \times \prod_{S=1}^{N} P(\mu_S | \theta_S, \tau_S^{-1}) \times$$

$$\prod_{S=1}^{N} P\left(\Sigma_S | \Omega_S, \rho_S\right) \times P\left(Z_j | \mu_j^Z, \Sigma^Z\right) \times P\left(\Sigma^Z | \Omega, \rho\right) \times P\left(\phi | \mu_\phi, \tau_\phi\right) \times P(\mu_\phi) \times P(\tau_\phi)$$

(eq.10)

As the joint posterior of all parameters is complex and high-dimensional, we cannot directly obtain posterior distribution functions, but the Bayesian model thus defined can be analyzed using Markov Chain Monte Carlo (MCMC); we have used the WinBUGS package (Lunn et al., 2000) to derive parameter estimates. MCMC methods require that the chain reaches a steady state, and the number of runs required to reach this state is considered as burn in. The model was run by taking 50,000,000 times from the posterior distribution from the sand dune and source samples, and the first 5,000,000 runs were considered as burn in. The large number of iterations was used to ensure convergence, despite the model's complexity and high dimensionality; the model converged during the run, as assessed by trace plots of simulations, Monte Carlo error and autocorrelation.

[Approx. location of Figure 4]

3. Results

Grain size data are presented in Table 1 to enable consideration of potential sorting effects during aeolian transportation. The sources reveal very similar physical grain sizes, and it is worth noting that whilst the Qc unit is mapped as a 'clay flat', the sediment sampled for analysis is dominantly sand. The erg, on the other hand, as might be expected as a result of aeolian transport and deposition is better sorted, and less enriched in the coarse and very coarse sand fraction. The individual dune sand samples retain marked variability, with the very-fine (62.5-150 μm) fraction ranging from 37% to 65%, and a single sample (8) retaining a substantial coarse (> 600 μm) component.

The Kruskal-Wallis H test (i.e. one-way ANOVA) was performed on geological units Egm, Qc and Qt2. Results identified 25 significant tracers between these groups (Table 2). Tracers that failed this test ($p > 0.05$) were removed. These were: Nd, Sm, Gd, Tb, Dy, Yb, Lu, (Nd/Yb), $(Gd/Yb)_n$, $(La/Sm)_n$, V, Cr, Co, Ni, Cu, Zn, Y, Zr, Nb, Ta, U, As, Bi, Cd, Ge, In, Mo, Sb, Se, Te, W, Mn, Si, ^{143}Nd, ^{144}Nd and ^{86}Sr. Whilst the successful discrimination of different tracers between geological units will vary when this method is applied to settings other than this location, the presence of 25 tracers with significant discriminatory power suggests that this method may be applicable in diverse geological settings and/or areas with contrasting weathering regimes.

[Approx. location of Table 2]

According to the DFA, a total of six individual tracer properties (Rb, Sr, ^{87}Sr, $(La/Yb)_n$, Ga and δCe) were selected for the optimum composite fingerprint, which correctly discriminated 81.6% of the source type samples (Figure 5).

[Approx. location of Table 3]

[Approx. location of Figure 5]

Although DFA results suggested that good source discrimination was achieved, with clear separation of the three group centroids, samples sourced from Qc were found to slightly overlap with the Qt2 source when the first two discriminant functions were plotted, and, to a lesser degree Qt2 and Egm also overlap slightly (Figure 5). The mean and SD of six optimum composite fingerprints that were selected for the Bayesian mixing model, are presented in Table 3. These were tested for normality via Wilks-Shapiro tests (Table 4), and the raw data revealed that the Sr and δCe tracers did not follow a normal distribution for all settings. To account for this, Box-Cox transformations (Box and Cox, 1964) were applied to all data, and the transformed data were used for model experimentation.

[Approx. location of Table 4]

The derived source contributions for the eight sand dune samples are presented in Table 5 and Figure 6. Overall, the alluvial fans and terraces (Qt2) provide the most abundant supply of sands (mean contribution across all 8 samples = 45.4%, and locally up to 92.7%), with the clay pans (Qc) and Eocene marls (Egm) each contributing around a quarter of the net sediment aeolian flux. However, the composition of the dune sands is highly variable, with different samples dominated

by different contributing sources, and locally, all three of the potential sources occur as both maxima and minima.

[Approx. location of Figure 6]

4. Discussion

4.1 Development of a Bayesian mixing model to discriminate aeolian sediment pathways

The mixing model to fingerprint aeolian sediment sources deployed in this study used composite signature comprising a suite of six geochemical characteristics (Rb, Sr, ^{87}Sr, La:Yb, Ga and δCe) identified by stepwise DFA as the most appropriate, and was able to account for >82% of the variance between the three sources. The suite of properties selected by the DFA method most likely reflects two principal factors; the ultimate source of the sediments, and the degree of weathering. The latter might well have variable influence across the source areas, and hence there is some overlap between samples of each class. High La:Yb ratios, for instance, are typically associated with deep igneous lithogenesis (Deffant and Drummond, 1990) and may locally reflect differing sediment contributions from the Precambrian crystalline basement provinces of central Iran. δCe, similarly, is often associated with intrusive igneous rocks, although may also be enriched in some sedimentary rocks (Wedepohl, 1978); in this study, the highest concentrations are found in the alluvial fans derived from the adjacent igneous mountains, but the second highest concentrations are found in the sedimentary marls of the Egm unit (Figure 2). In short, the highly varied geology of central Iran, ranging from Precambrian magmatic

rocks to Cenozoic marine sediments, promotes a high degree of variance in the geochemical fingerprint of modern aeolian sediments. Compounding this is the range of weathering intensities seen, from the intense weathering history of the sediments of Quaternary clay pans, to the more moderate weathering of the sands of the alluvial fans forming the piedmonts of the neighbouring ranges.

4.2 Potential for application to other aeolian depositional settings

Despite the usefulness of understanding the provenance of aeolian sands, the sophistication of unmixing models within the aeolian science community generally lags that of fluvial science, in particular in terms of the numerical underpinning of methods applied. Indeed, many such studies attempt to derive provenance estimates only qualitatively (e.g. Fitzsimmons et al, 2009), or, in the few recent cases where robust unmixing models have been applied, relatively simple approaches to incorporating uncertainty into models have been taken (e.g. Liu et al., 2016).

The successful application of a Bayesian model within an MCMC framework to aeolian sands of a small erg in this study demonstrates the potential of this approach more widely. It is particularly likely to complement detrital zircon U-Pb dating provenance studies, and may prove especially useful in settings where there are insufficient zircon grains to enable the application of this method (e.g. Jia et al., 2015, Nie and Peng, 2014, Ren et al., 2014, Thorpe et al., 1992). Further application of the methods demonstrated here is required to test the ability of such methods globally, but these results suggest a promising future, and a new direction for aeolian provenance studies. For instance, it would be useful to explore the power of these methods in larger-scale settings, such as the continental dunefields of southern Africa and Australia, where provenance studies have been used to explore the

relationship between tectonic setting and sedimentation (e.g. Garzanti et al., 2014) and explore the long-term evolution of landscapes (e.g. Pell et al., 1997; 2000). This will also elucidate the importance of diversity of local geology and weathering regimes in producing sufficiently distinctive fingerprints.

Accurate propagation of the uncertainties associated with the component contributions is also a valuable aspect of the methodology employed here and allows more realistic interpretation of the data. For instance, the most abundant two source components of samples E (Qt2 = 62.3%; Qc = 23%) and D (Egm = 56.3%; Qc = 28.7%) might suggest similar proportions of the major components at these dunes; roughly 60:25. However, consideration of the lower confidence of the fingerprint of sample D (Figure 6) reveals that whilst the composition of this sample is much more open to interpretation, sample E is quite clearly dominated by the alluvial fan-derived sands (Qt2).

4.3 Implications for aeolian sediment transport pathways

Overall, the surrounding Quaternary fans and terraces contribute most (~45%) to the composition of Ashkzar erg; yet this is a disproportionately low value, given that they represent 78% of the surrounding area. Conversely, the size of the overall contributions from the Quaternary clay flats (~26%) and Eocene marls (~28%) to the samples studied reveals the importance of these landscape units as sediment sources, given that these units occupy only 13% and 7% of the surrounding area, respectively. The importance of the marls as a source sediment, which outcrop only to the north of the Ashkzar dunefield, suggests that net wind regime alone cannot be considered as indicative of the net sediment transport in the region (Figure 1), as

westerly winds are equally strong here yet import much less sediment. Both the wind regime and potential sediment sources must be considered when evaluating net aeolian sediment flux.

There is much spatial variation in the composition of the dune sands of Ashkzar erg (Figure 6). Even before the geochemical composition of these sands in considered, such variability is evident from the differing grain size profiles in the eight samples investigated here (Table 1). Sample G, from the far south of the dunefield, contains ~20% coarse sands (defined here as > 600 μm), an unusually high figure for an aeolian dune, although this sample is taken close to the border with the mapped region of slipfaceless dome dunes, which tend to accumulate from coarser sands (Lancaster, 1995). That said, sample H, from within the dome dunes, is not unusually coarse.

Broadly, and considering the uncertainties presented by the methodology proposed herein, two groups can be discerned within the samples geochemically analysed for provenance (Figure 6). Samples taken from along the south and west of the dunefield (B, E, F and G) are dominated to varying degrees by sediment from the surrounding Quaternary fans and terraces (i.e. source unit Qt2), whereas most samples to the north and east (A, D and H) show much greater contributions from the Eocene marls (Egm) and clay flats (Qc). However, the division is not clear-cut; sample C, in the northeast of the dunefield, has a dominant component from the Qt2 unit (with the second component only very slightly overlapped at 2σ confidence levels).It is, perhaps, unsurprising that the more northerly samples tend to show an increased input from the Eocene marls (Egm), as these units have been shown to contribute disproportionately to the sediment flux in the area, and also outcrop exclusively on the northern side of the valley (Figure 1).

The provenance of the sands is even less readily correlated with dune morphology, with the Qt2-dominated sands occurring within three defined dune morphological zones (barchans, barchanoid ridges and asymmetrical barchans). Samples A and B, the closest pair of samples studied (~2.2 km apart), yield very different provenance fingerprints, despite both lying within the region of Ashkzar erg dominated by barchanoid ridges. The overall morphology of the dunes (Figure 3) supports spatially and /or temporally variable sediment availability, with the transformation of barchans to barchanoid ridges essentially being sediment-supply controlled, and asymmetric barchan/linear forms believed to be the result of asymmetries of sediment supply, or changes to the wind regime (Bagnold, 1941; Lancaster 1995).

The heterogeneity in the sediment provenance evident here suggests that either a) some kind of fractionation of the aeolian sediment flux is occurring, with different sources depositing sediment at different locations or b) different sediment transport pathways have been active intermittently and asynchronously during the formation of the dunefield. The similar physical composition (i.e. grain size) of the sources, and the lack of evidence of systematic variation across the dunefield, would tend to support the latter suggestion. Different sediment pathways might result from different sources become more or less active over time, or might result from changing wind regime over long (i.e. late Quaternary) timescales. The heterogeneity evident also suggests that during dune accumulation periods, large-scale mixing of aeolian sands from different sources (which might be expected given transport distances of 10-50 km) is not occurring. In the absence of any chronological control for these dunes, such hypotheses cannot be conclusively tested currently, but establishing the relative roles of spatial and temporal variability in dune accumulation would be a worthwhile exercise.

5. Conclusion

In dryland environments, understanding the main sources for aeolian sediments is an essential step in developing management strategies to reduce aeolian sediment loadings and wind erosion. Establishing aeolian sediment pathways, however, is not usually straightforward and is complicated when multiple potential source areas might contribute to a region of net sand accumulation. The method proposed here, based on methodologies applied to fluvial sediments, uses a suite of geochemical data to identify the most apposite characteristics (the 'fingerprint') for discerning superficially similar sources of aeolian sediment. Whereas these methods have become widely adopted in fluvial geomorphology and catchment science over the past two decades, they remain almost unused in aeolian science. Here, it has been successfully demonstrated on fine sand in a small dunefield in central Iran, but it might be applied equally to dust (i.e. silt) flux, although longer transport distances are liable to prove more difficult to fingerprint unless relatively discrete and distinct sources can be identified. The use of MCMC methods to provide confidence estimates in the mixing model output enables more rigorous interpretation of the relative importance of different sediment sources.

This method revealed within Ashkzar erg unexpected spatial heterogeneity of dune composition (and thus provenance), which has a complex relationship with the position within the dunefield, the dune type and other physical characteristics. The Eocene marls in the surrounding area have been shown to contribute disproportionately to the sediments of the dunes. In terms of management of sand and dust hazard at this location, both the original source areas and those parts of the

dunefield enriched in the Egm component might be viewed as priority targets for landscape stabilization efforts, due to their apparent propensity for aeolian mobilization.

More widely, the methods proposed here for aeolian provenance unmixing method can be applied to any mixed-source aeolian sediment to elucidate differing susceptibilities to aeolian deflation, and reveal transport pathways at timescales longer than those possible by either field study or remote sensing. Disciplines which might benefit from the adoption of such methods include not just aeolian geomorphology, but also dryland land management, soil science, engineering geology and potentially palaeoenvironmental and palaeoclimatological studies. A combination of the methods presented herein with geochronological studies may enable calculation of flux rates to provide quantification of long-term sediment fluxes, even when, as is very often the case with aeolian sediments, transport pathways are complex and multi-phase.

References

Amiraslani, F. and Dragovich, D. (2011). Combating desertification in Iran over the last 50 years: An overview of changing approaches. *Journal of Environmental Management* 92 (1), 1-13. doi: 10.1016/j.jenvman.2010.08.012.

Bagnold, R.A. 1941. The physics of blown sand. Methuen, London.

Box, G.E.P & Cox, D.R. (1964). An analysis of transformations. *Journal of the Royal Statistical Society, Series B*. 26 (2): 211–252.

Brewer, M. J., Filipe, J. A. N., Elston, D. A., Dawson, L. A., Mayes, R. W., Soulsby, Ch., & Dunn, S. M. (2005). A Hierarchical Model for Compositional Data Analysis. *Journal of Agricultural, Biological, and Environmental Statistics*, *10*(1), 19–34. doi:10.1198/108571105X28200

Chen, F., Fang, N., & Shi, Z. (2016). Using biomarkers as fi ngerprint properties to identify sediment sources in a small catchment. *Science of the Total Environment*, *557-558*, 123–133. doi:10.1016/j.scitotenv.2016.03.028

Collins, A. L., & Walling, D. E. (2007). Sources of fine sediment recovered from the channel bed of lowland groundwater-fed catchments in the UK. *Geomorphology*, *88*, 120–138. doi:10.1016/j.geomorph.2006.10.018

Collins, A. L., Zhang, Y., McChesney, D., Walling, D. E., Haley, S. M., & Smith, P. (2012). Sediment source tracing in a lowland agricultural catchment in southern England using a modified procedure combining statistical analysis and numerical modelling. *Science of the Total Environment*, *414*, 301–317. doi:10.1016/j.scitotenv.2011.10.062

Collins, A. L., Zhang, Y. S., Duethmann, D., Walling, D. E., & Black, K. S. (2013). Using a novel tracing-tracking framework to source fine-grained sediment loss to watercourses at sub-catchment scale. *Hydrological Processes*, *27*(6), 959–974. doi:10.1002/hyp.9652

Collins, A. L., Zhang, Y., Walling, D. E., Grenfell, S. E., & Smith, P. (2010). Tracing sediment loss from eroding farm tracks using a geochemical fingerprinting procedure combining local and genetic algorithm optimisation. *Science of the Total Environment*, *408*(22), 5461–5471. doi:10.1016/j.scitotenv.2010.07.066

Collins, A. L., Zhang, Y., Walling, D. E., Grenfell, S. E., Smith, P., Grischeff, J., … Brogden, D. (2012). Quantifying fine-grained sediment sources in the River Axe catchment, southwest England: Application of a Monte Carlo numerical modelling framework incorporating local and genetic algorithm optimisation. *Hydrological Processes*, *26*(13), 1962–1983. doi:10.1002/hyp.8283

Collins, A.L., Pulley, S., Foster, I.D.L., Gellis A., Porto, P., Horowitz, A.J. (2016). Sediment source fingerprinting as an aid to catchment management: A review of the current state of knowledge and a methodological decision-tree for end-users. *Journal of Environmental Management*, 194, 86–108. doi.org/10.1016/j.jenvman.2016.09.075

Cooper RJ and Krueger T (2017, in press). An extended Bayesian sediment fingerprinting mixing model for the full Bayes treatment of geochemical uncertainties. *Hydrological Processes*. DOI: 10.1002/hyp.11154.

Cooper, R. J., Krueger, T., Hiscock, K. M., & Rawlins, B. G. (2014). Sensitivity of fluvial sediment source apportionment to mixing model assumptions : A Bayesian model comparison. *Water Resources Research*, 9031–9047. doi:10.1002/2014WR016194.

Cooper, R. J., Krueger, T., Hiscock, K. M., & Rawlins, B. G. (2015). High-temporal resolution fluvial sediment source fingerprinting with uncertainty: A Bayesian approach. *Earth Surface Processes and Landforms*, *40*(1), 78–92. doi:10.1002/esp.3621

Daga, R., Ribeiro Guevara, S., Sánchez, M. L., & Arribére, M. (2008). Source identification of volcanic ashes by geochemical analysis of well preserved

lacustrine tephras in Nahuel Huapi National Park. *Applied Radiation and Isotopes*, *66*(10), 1325–1336. doi:10.1016/j.apradiso.2008.03.009

Defant, M.J. and Drummond, M.S. 1990. Derivation of some modern arc magmas by melting of young subducted lithosphere. *Nature* 367, 662–665

Delmonte, B., Baroni, C., Andersson, P.S., Schoberg, H., Hansson, M., Aciego, S., Petit, J.-R., Albani, S., Mazzola, C., Maggi, V., Frezzotti, M., 2010. Aeolian dust in the Talos Dome ice core (East Antarctica, Pacific/Ross Sea sector): Victoria Land versus remote sources over the last two climate cycles. *Journal of Quaternary Science* 25, 1327-1337.

Delmonte, B., Basile-Doelsch, I., Petit, J.R., Maggi, V., Revel-Rolland, M., Michard, A., Jagoutz, E., Grousset, F., 2004. Comparing the Epica and Vostok dust records during the last 220,000 years: stratigraphical correlation and provenance in glacial periods. *Earth-Science Reviews* 66, 63-87.

Dou, Y., Yang, S., Liu, Z., Clift, P. D., Shi, X., Yu, H., & Berne, S. (2010). Provenance discrimination of siliciclastic sediments in the middle Okinawa Trough since 30ka: Constraints from rare earth element compositions. *Marine Geology*, *275*(1-4), 212–220. doi:10.1016/j.margeo.2010.06.002

Douglas, G., Caitcheon, G., & Palmer, M. (2009). Sediment source identification and residence times in the Maroochy River estuary, southeast Queensland, Australia. *Environmental Geology*, *57*(3), 629–639. doi:10.1007/s00254-008-1336-7

Egozcue, J. J., Pawlowsky-Glahn, V., Mateu-Figueras, G., & Barceló-Vidal, C. (2003). Isometric Logratio Transformations for Compositional Data Analysis.

Mathematical Geology, *35*(3), 279–300. doi:10.1023/A:1023818214614

Fox, J. F., & Papanicolaou, A. N. (2008). An un-mixing model to study watershed erosion processes. *Advances in Water Resources*, *31*, 96–108. doi:10.1016/j.advwatres.2007.06.008

Garzanti, E., Vermeesch, P., Ando, S., Vezzoli, G., Valagussa, M., Allen, K., Kadi, K.A., Al-Juboury, A.I.A., 2013. Provenance and recycling of Arabian desert sand. *Earth-Science Reviews*. 120, 1-19.

Garzanti, E., Vermeesch, P., Padoan, M., Resentini, A., Vezzoli, G., Ando, S., 2014. Provenance of Passive-Margin Sand (Southern Africa). *Journal of Geology*, 122(1), 17-42. doi:10.1086/674803

Gellis, A. C., & Noe, G. B. (2013). Sediment source analysis in the Linganore Creek watershed, Maryland, USA, using the sediment fingerprinting approach: 2008 to 2010. *Journal of Soils and Sediments*, 13(10), 1735–1753. doi:10.1007/s11368-013-0771-6

Haddadchi, A, Ryder, D.S., Evrard, O., Olley, J. (2013). Sediment fingerprinting in fluvial systems: review of tracers, sediment sources and mixing models. *Int. J. Sediment Res.*, 28, 560–578

Huntsman-Mapila, P., Kampunzu, A.B., Vink, B., Ringrose, S., 2005. Cryptic indicators of provenance from the geochemistry of the Okavango Delta sediments, Botswana. *Sedimentary Geology* 174, 123-148.

Honda, M., Yabuki, S., & Shimizu, H. S. H. I. (2004). Geochemical and isotopic studies of aeolian sediments in China. *Sedimentology*, 211–230. doi:10.1046/j.1365-3091.2003.00618.x

Jia, Y., Fu, B., Jolivet, M. and Zheng, S. Cenozoic tectono-geomorphological growth of the SW Chinese Tian Shan: insight from AFT and detrital zircon U-Pb data. *Journal of Asian Earth Sciences*, 2015, 111, 395-413.

Koiter, A. J., Owens, P. N., Petticrew, E. L., & Lobb, D. A. (2013). The behavioural characteristics of sediment properties and their implications for sediment fingerprinting as an approach for identifying sediment sources in river basins. *Earth-Science Reviews*, *125*, 24–42. doi:10.1016/j.earscirev.2013.05.009

Lancaster, N. 1995.Geomorphology of Desert Dunes. Routledge, London.

Lin, J., Huang, Y., Wang, M. kuang, Jiang, F., Zhang, X., & Ge, H. (2015). Assessing the sources of sediment transported in gully systems using a fingerprinting approach: An example from South-east China. *Catena*, *129*, 9–17. doi:10.1016/j.catena.2015.02.012

Liu, B.L., Niu, Q.H., Qu, J.J., Zu, R.P. (2016). Quantifying the provenance of aeolian sediments using multiple composite fingerprints. *Aeolian Research*, 22, 117-122. doi:10.1016/j.aeolia.2016.08.002

Lunn, D.J., Thomas, A., Best, N., and Spiegelhalter, D. (2000) WinBUGS -- a Bayesian modelling framework: concepts, structure, and extensibility. *Statistics and Computing*, 10:325--337.

Martínez-Carreras, N., Udelhoven, T., Krein, A., Gallart, F., Iffly, J. F., Ziebel, J. and Walling, D. E. (2010). The use of sediment colour measured by diffuse reflectance spectrometry to determine sediment sources : Application to the Attert River catchment. *Journal of Hydrology*, *382*(1-4), 49–63. doi:10.1016/j.jhydrol.2009.12.017

Massoudieh, A., Gellis, A., Banks, W. S., & Wieczorek, M. E. (2013). Suspended sediment source apportionment in Chesapeake Bay watershed using Bayesian chemical mass balance receptor modeling. *Hydrological Processes*, *27*(24), 3363–3374. doi:10.1002/hyp.9429

Motha, J. A., Wallbrink, P. J., Hairsine, P. B., & Grayson, R. B. (2003). Determining the sources of suspended sediment in a forested catchment in southeastern Australia. *Water Resources Research*, *39*(3), 1056. doi:10.1029/2001wr000794

Muhs, D. R., Lancaster, N. and Skipp, G.L. (2017). A complex origin for the Kelso Dunes, Mojave National Preserve, California, USA: A case study using a simple geochemical method with global applications. Geomorphology, 276, 222-243. doi: 10.1016/j.geomorph.2016.10.002

Mukundan, R., Walling, D. E., Gellis, A. C., Slattery, M. C., & Radcliffe, D. E. (2012). Sediment Source Fingerprinting: Transforming From a Research Tool to a Management Tool. *Journal of the American Water Resources Association*, *48*(6), 1241–1257. doi:10.1111/j.1752-1688.2012.00685.x

Naddafi, K., Nabizadeh, R., Soltanianzadeh, Z., Ehrampoosh, M.H., 2006. Evaluation of dustfall in the air of Yazd. *Journal of Environmental Health Science and Engineering*, 3, 161-168.

Nanson, G.C., Chen, X.Y., Price, D.M. (1995). Aeolian and fluvial evidence of changing climate and wind patterns during the past 100 Ka in the Western Simpson Desert, Australia. *Palaeogeography Palaeoclimatology Palaeoecology* 113, 87-102.

Nie, J. and Peng, W. (2014). Automated SEM–EDS heavy mineral analysis reveals

no provenance shift between glacial loess and interglacial paleosol on the Chinese Loess Plateau. *Aeolian Research* 13, 71-75.

Nosrati, K., Govers, G., Semmens, B. X., & Ward, E. J. (2014). A mixing model to incorporate uncertainty in sediment fingerprinting. *Geoderma 217-218*, 173–180. doi:10.1016/j.geoderma.2013.12.002

Owens, P.N., Blake, W.H., Gaspar, L., Gateuille, D., Koiter, A.J., Lobb, D.A., Petticrew, E.L., Reiffarth, D.G., Smith, H.G. & Woodward, J.C. (2016). Fingerprinting and tracing the sources of soils and sediments: Earth and ocean science, geoarchaeological, forensic, and human health applications. *Earth-Science Reviews*, 162, 1-23. doi: 10.1016/j.earscirev.2016.08.012

Palmer, M. J., & Douglas, G. B. (2008). A Bayesian statistical model for end member analysis of sediment geochemistry, incorporating spatial dependences. *Journal of the Royal Statistical Society. Series C: Applied Statistics 57*(3), 313–327. doi:10.1111/j.1467-9876.2007.00615.x

Parnell, A. C., Phillips, D. L., Bearhop, S., Semmens, B. X., Ward, E. J., Moore, J. W., Inger, R. (2013). Bayesian stable isotope mixing models. *Environmetrics 24*(6), 387–399. doi:10.1002/env.2221

Pell, S.D., Williams, I.S., Chivas, A.R., 1997. The use of protolith zircon-age fingerprints in determining the protosource areas for some Australian dune sands. *Sedimentary Geology* 109, 233-260.

Pell, S.D., Chivas, A.R., Williams, I.S. 2000. The Simpson, Strzelecki and Tirari Deserts: development and sand provenance. Sedimentary Geology 130 (1-2), 107–130. doi: 10.1016/S0037-0738(99)00108-6

Pethierick, L., McGowan, H., Moss, P., 2008. Climate variability during the Last Glacial Maximum in eastern Australia: evidence of two stadials? *Journal of Quaternary Science* 23, 787-802.

Pittam, N. J., Foster, I. D. L., & Mighall, T. M. (2009). An integrated lake-catchment approach for determining sediment source changes at Aqualate Mere, Central England. *Journal of Paleolimnology*, *42*(2), 215–232. doi:10.1007/s10933-008-9272-9

Rao, W., Tan, H., Jiang, S., & Chen, J. (2011). Trace element and REE geochemistry of fine- and coarse-grained sands in the Ordos deserts and links with sediments in surrounding areas. *Chemie Der Erde - Geochemistry*, *71*(2), 155–170. doi:10.1016/j.chemer.2011.02.003

Ren, R., Han, B-F., Xu, Z. and Li, Q. 2014. When did the subduction first initiate in the southern Paleo-Asian Ocean: New constraints from a Cambrian intra-oceanic arc system in West Junggar, NW China. *Earth and Planetary Science Letters* 388, 222–236

Semmens, B. X., Moore, J. W., & Ward, E. J. (2009). Improving Bayesian isotope mixing models: A response to Jackson et al. (2009). *Ecology Letters*, *12*(3), 10–12. doi:10.1111/j.1461-0248.2009.01283.x

Sherriff, S. C., Franks, S. W., Rowan, J. S., Fenton, O., & Ó'hUallacháin, D. (2015). Uncertainty-based assessment of tracer selection, tracer non-conservativeness and multiple solutions in sediment fingerprinting using synthetic and field data. *Journal of Soils and Sediments*, *15*(10), 2101–2116. doi:10.1007/s11368-015-1123-5

Smith, H. G., & Blake, W. H. (2014). Sediment fingerprinting in agricultural catchments: A critical re-examination of source discrimination and data corrections. *Geomorphology*, *204*, 177–191. doi:10.1016/j.geomorph.2013.08.003

Stewart, H. A., Massoudieh, A., & Gellis, A. (2015). Sediment source apportionment in Laurel Hill Creek, PA, using Bayesian chemical mass balance and isotope fingerprinting. *Hydrological Processes*, *29*(11), 2545–2560. doi:10.1002/hyp.10364

Stone, M., Collins, A. L., Silins, U., Emelko, M. B., & Zhang, Y. S. (2014). The use of composite fingerprints to quantify sediment sources in a wildfire impacted landscape, Alberta, Canada. *Science of the Total Environment*, *473-474*, 642–650. doi:10.1016/j.scitotenv.2013.12.052

Thorpe, R.I., Hickman, A.H., Davis, D.W., Mortensen, J.K. and Trendall, A.F., 1992. U/Pb zircon geochronology of Archaean felsic units in the Marble Bar region, Pilbara Craton, Western Australia. *Precambrian Research*, 56, 169-189.

Vale, S. S., Fuller, I. C., Procter, J. N., Basher, L. R., & Smith, I. E. (2016). Characterization and quantification of suspended sediment sources to the Manawatu River, New Zealand. *Science of The Total Environment*, *543*, 171–186. doi:10.1016/j.scitotenv.2015.11.003

Voli, M. T., Wegmann, K. W., Bohnenstiehl, D. R., Leithold, E., Osburn, C. L., & Polyakov, V. 2013. Fingerprinting the sources of suspended sediment delivery to a large municipal drinking water reservoir: Falls Lake, Neuse River, North Carolina, USA. *Journal of Soils and Sediments*, *13*(10), 1692–1707.

doi:10.1007/s11368-013-0758-3

Walling, D.E., Collins, A.L., & Stroud, R.W. 2008. Tracing suspended sediment and particulate phosphorus sources in catchments. *Journal of Hydrology*, *350*(3-4), 274–289. doi:10.1016/j.jhydrol.2007.10.047

Walling, D.E. 2013. The evolution of sediment source fingerprinting investigations in fluvial systems. Journal of Soils and Sediments, 13(10), 1658-1675. doi: 10.1007/s11368-013-0767-2

Wasklewicz, T.A., Meek, N., 1995. Provenance of aeolian sediment: The upper Coachella Valley, California. *Physical Geography* 16, 539-556.

Wilkinson, S.N., Hancock, G.J., Bartley, R., Hawdon, A.A., & Keen, R.J. (2013). Using sediment tracing to assess processes and spatial patterns of erosion in grazed rangelands, Burdekin River basin, Australia. *Agriculture, Ecosystems and Environment*, *180*, 90–102. doi:10.1016/j.agee.2012.02.002

Wilson, C.G., Papanicolaou, A.N.T., & Denn, K.D. (2012). Partitioning fine sediment loads in a headwater system with intensive agriculture. *Journal of Soils and Sediments*, *12*(6), 966–981. doi:10.1007/s11368-012-0504-2

Winspear, N.R., Pye, K., 1996. Textural, geochemical and mineralogical evidence for the sources of aeolian sand in central and southwestern Nebraska, USA. Sedimentary Geology 101, 85-98.

Yang, X., Liu, Y., Li, C., Song, Y., Zhu, H., Jin, X., 2007. Rare earth elements of aeolian deposits in Northern China and their implications for determining the provenance of dust storms in Beijing. *Geomorphology* 87, 365-377.

739

740

741

742 Tables

743 Table 1

		Grain size (μm)					
		<62.5	62.5 - 150	150 - 300	300 - 600	600 - 1180	1180 - 1700
Mean Eocene marl (Egm) source (% ± 1σ)		3.0 ± 1.4	40.2 ± 10.6	20.0 ± 6	15.1 ± 4.2	15.6 ± 6.7	6.1 ± 5
Mean Quaternary clay flat (Qc) source (% ± 1σ)		3.1 ± 1.3	29.4 ± 9.2	21.8 ± 5.6	19.0 ± 3.9	19.7 ± 8.1	6.9 ± 4
Mean Quaternary terrace/fan (Qt2) source (% ± 1σ)		2.2 ± 2.3	34.7 ± 7.3	20.4 ± 5.6	17.1 ± 3.9	19.3 ± 5.3	6.4 ± 2
Mean Ashkzar erg dune sands (% ± 1σ)		1.1 ± 0.9	47.8 ± 9.3	29.7 ± 8.4	17.4 ± 13.9	3.4 ± 5.4	0.6 ± 1.3
Ashkzar erg dune samples (%)	A	0.3	57.6	38.2	3.4	0.5	0.0
	B	0.5	41.0	18.1	39.0	1.4	0.0
	C	2.1	43.9	16.7	35.9	1.4	0.0
	D	0.5	42.5	34.0	22.0	1.0	0.0
	E	2.7	51.8	31.2	7.9	5.0	1.4
	F	1.0	64.5	32.0	2.5	0.0	0.0
	G	1.0	36.8	28.0	14.4	16.2	3.6
	H	0.6	44.6	39.3	13.7	1.8	0.0

744

Table 2

Fingerprint property	Chi square	p value	Fingerprint property	Chi square	p-value
La	6.669	0.036*	Y	4.151	0.125
Ce	7.476	0.024*	Zr	3.744	0.154
Pr	9.552	0.008**	Nb	0.582	0.748
Nd	0.415	0.813	Hf	16.1	<0.001***
Sm	0.081	0.96	Ta	4.922	0.085
Eu	10.23	0.006**	Th	10.28	0.006**
Gd	0.434	0.805	U	4.8	0.091
Tb	0.017	0.992	As	5.166	0.076
Dy	1.359	0.507	Bi	0.725	0.695
Ho	8.067	0.018*	Cd	0.111	0.946
Er	9.257	0.01*	Ga	13.4	<0.001***
Tm	8.373	0.015*	Ge	0.59	0.745
Yb	1.026	0.599	In	1.215	0.545
Lu	0.104	0.949	Li	7.213	0.027*
∑REE	7.086	0.029*	Mo	0.227	0.893
Eu/Eu*	10.23	0.006**	P	13.05	<0.001***
(Nd/Yb)	0.785	0.675	S	16.36	<0.001***
$(Gd/Yb)_n$	0.729	0.695	Sb	1.409	0.494
$(La/Yb)_n$	13.89	0.001**	Se	0.858	0.651
$(La/Sm)_n$	4.725	0.094	Sn	6.466	0.039*
$(La/Lu)_n$	12.78	0.002**	Te	4.685	0.096
δCe	5.435	0.041*	Ti	6.56	0.038*
Rb	15.18	<0.001***	Tl	6.614	0.037*
Sr	16.44	<0.001***	W	0.086	0.958
Ba	6.379	0.041*	Mn	1.673	0.433
V	3.083	0.214	Si	0.342	0.843
Cr	5.359	0.069	^{143}Nd	1.042	0.534
Co	1.271	0.53	^{144}Nd	2.031	0.362
Ni	3.998	0.135	^{86}Sr	5.754	0.056
Cu	3.18	0.204	^{87}Sr	7.124	0.028*
Zn	0.236	0.889			

Table 3

		Optimum composite fingerprints					
Sediment	Tracer	Rb	Sr	^{87}Sr	$(La/Yb)_n$	Ga	δCe
Sand dune	Mean	7.8	144	85	7.1	1.2	0.69
	SD	0.74	18.6	28	0.54	0.11	0.020
Source	Tracer	Rb	Sr	^{87}Sr	$(La/Yb)_n$	Ga	δCe
Egm	Mean	8.9	293	82	6.9	1.3	0.70
	SD	2.3	192	31	0.58	0.29	0.085
Qc	Mean	10	139	91	7.4	1.1	0.69
	SD	2.6	36.5	31	0.54	0.27	0.071
Qt2	Mean	7.1	163	98	7.7	0.99	0.74
	SD	0.82	135	44	0.89	0.26	0.27

Table 4

		Tracer					
	Source	Rb	Sr	^{87}Sr	(La/Yb)n	Ga	δCe
Raw data	Egm	0.944	0.362	0.930	0.996	0.980	0.810
	Qc	0.347	0.734	0.486	0.794	0.900	0.167
	Qt2	0.983	0.019	0.182	0.557	0.710	0.013
		Tracer					
	Source	Rb	Sr	^{87}Sr	(La/Yb)n	Ga	δCe
Box-Cox transformed data	Egm	0.944	0.724	0.930	0.996	0.980	0.978
	Qc	0.347	0.931	0.486	0.794	0.900	0.542
	Qt2	0.983	0.085	0.182	0.557	0.710	0.061

Table 5

Sediment samples	Source	Mean (%)	SD (%)	MC error	Median	Percentile (2.5)	Percentile (97.5)
A	Egm	44.1	11.5	0.003	44.5	21	64.7
	Qc	39.8	11.2	0.003	37.9	22.7	65.8
	Qt2	16.2	8.3	0.001	15.2	3.6	34
B	Egm	32.6	7.3	0.002	33	18.2	46.2
	Qc	5.1	3.8	0.001	4.1	0.6	15
	Qt2	62.2	6	0.001	62.1	50.3	73.7
C	Egm	20.8	6.3	0.002	21	8.1	33
	Qc	27.5	6.5	0.002	26.6	17.1	43
	Qt2	51.6	5.2	0.000	51.1	42	62.5
D	Egm	56.3	13	0.004	56.9	29.9	79.4
	Qc	28.7	10.5	0.003	27	12.2	53.4
	Qt2	14.9	9.4	0.001	14.4	0.4	34.2
E	Egm	14.3	5	0.001	14.3	4.6	24.6

		Qc	23	5.3	0.001	22.3	14.2	35.1
		Qt2	62.6	4.8	0.000	62.7	52	71.9
	F	Egm	17.6	6.3	0.001	17.7	4.8	29.9
		Qc	32.4	7.4	0.002	31.5	20.4	49.6
		Qt2	49.9	5.5	0.001	49.4	39.7	61.5
	G	Egm	3.4	3.2	0.000	2.44	0.000	12.2
		Qc	3.9	3.9	0.000	2.6	0.000	14.7
		Qt2	92.7	6	0.001	94	78.2	99.7
	H	Egm	37.3	11.2	0.003	37.8	14.5	57.9
		Qc	49.7	12.6	0.004	47.7	30	79
		Qt2	13	8.6	0.001	12	0.4	31.5

753

754

Figure captions

Figure 1: Location and geological map of the Yazd-Ardekan Plain and sampling sites. Dominant and minor wind directions shown in Part C. Number of sampling points = 57. Qt2, Qc, Egm (potential sediment sources) and Qsd (sediment) represent young alluvial fans and terraces, clay flats, gypsiferous marl and sand dunes, respectively.

Figure 2: Source and sediment sink regions within the study area. Source regions include: a) clay flats (Qc); b) gypsiferous marl (Egm); and c) young alluvial fans and terraces (Qt2). Sediment sinks include: d) sand dunes (Qsd).

Figure 3. Morphological mapping of dune types within Ashkzar erg reveals the dominance of barchans and barchanoid ridges. There are less distinct zones within the dunefield in the north, where the interdunes are sandy and the transverse forms much less distinct, and in the far southeast, where patchy slipface-less dunes dominate. Base imagery is courtesy of Google Earth™, and letters refer to the eight samples analysed for physical and geochemical characteristics within the dunefield.

Figure 4: A directed acyclic graph of the Bayesian mixing model employed in this study.

Figure 5: Two-dimensional scatter plot of the first and second discriminant functions from stepwise DFA for the source groups Egm (Eocene gypsiferous marls), Qc (Quaternary clay flats) and Qt2 (Quaternary alluvial fans and terraces).

Figure 6: Source contributions for each aeolian sediment samples by Bayesian mixing model with 95% credible limits. Base imagery is courtesy of Google Earth™.

Table captions

Table 1: Grain size data for the source areas, the dunefield, and individual samples from within the dunefield.

Table 2: Kruskal-Wallis H test results for selecting fingerprint properties for distinguishing individual source types. Confidence is highlighted at >95% with a single asterisk, >99% with a double asterisk, and >99.9% with a triple asterisk.

Table 3: Summary geochemistry data for sand dune samples and potential sediment sources. All are reported to two significant figures, except Sr, which is reported to three, due to the larger magnitude of the concentrations.

Table 4: Normality tests on the raw data for the tracers selected for the fingerprint revealed that two tracers (Sr and δCe) were not normally distributed for the Qt2 unit; for this reason, Box-Cox transformations were performed on all data, which did provide normal distributions for all tracers.

Table 5. Estimated contribution from each source for aeolian sediment samples by Bayesian mixing model.

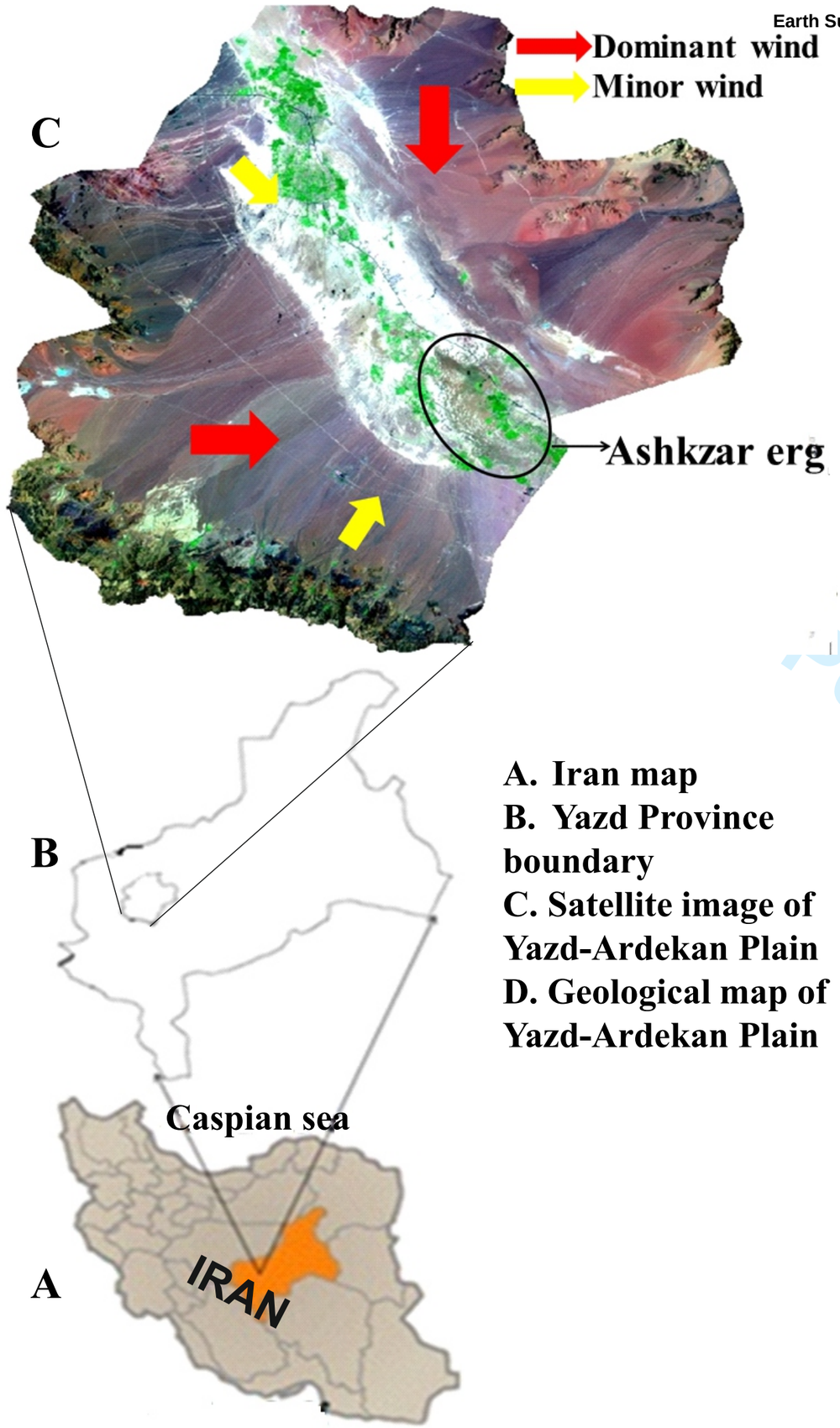

A. Iran map
B. Yazd Province boundary
C. Satellite image of Yazd-Ardekan Plain
D. Geological map of Yazd-Ardekan Plain

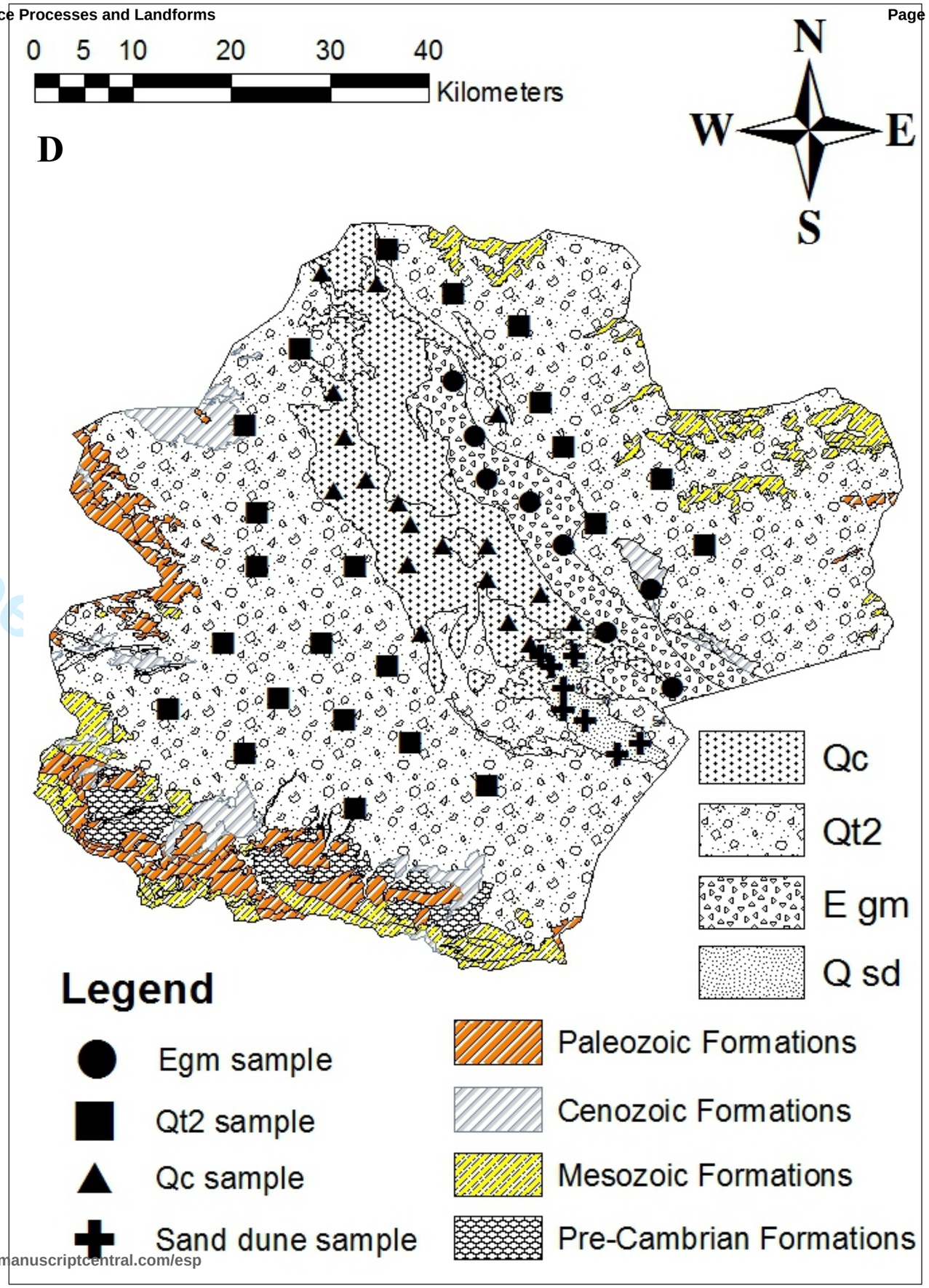

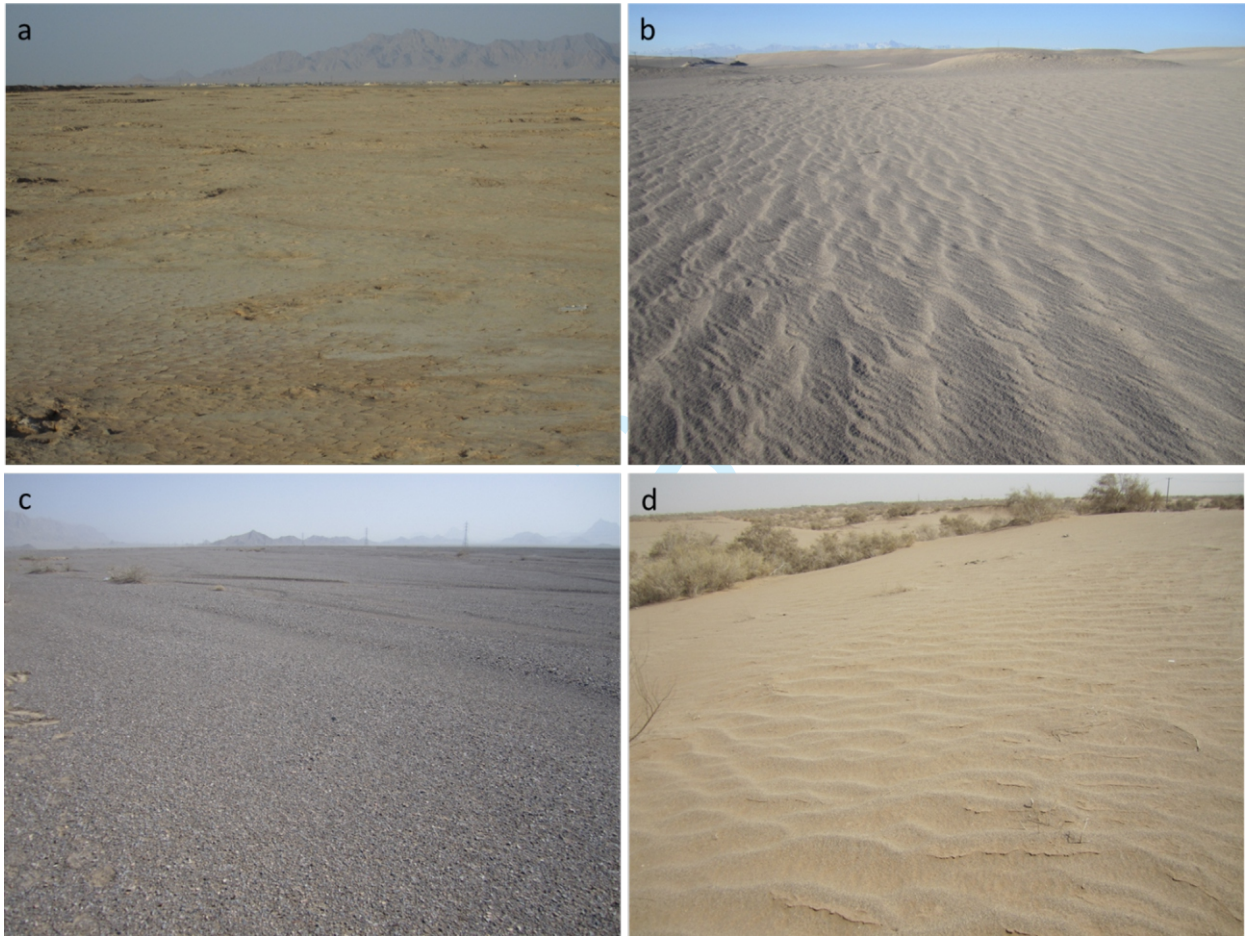
a
b
c
d

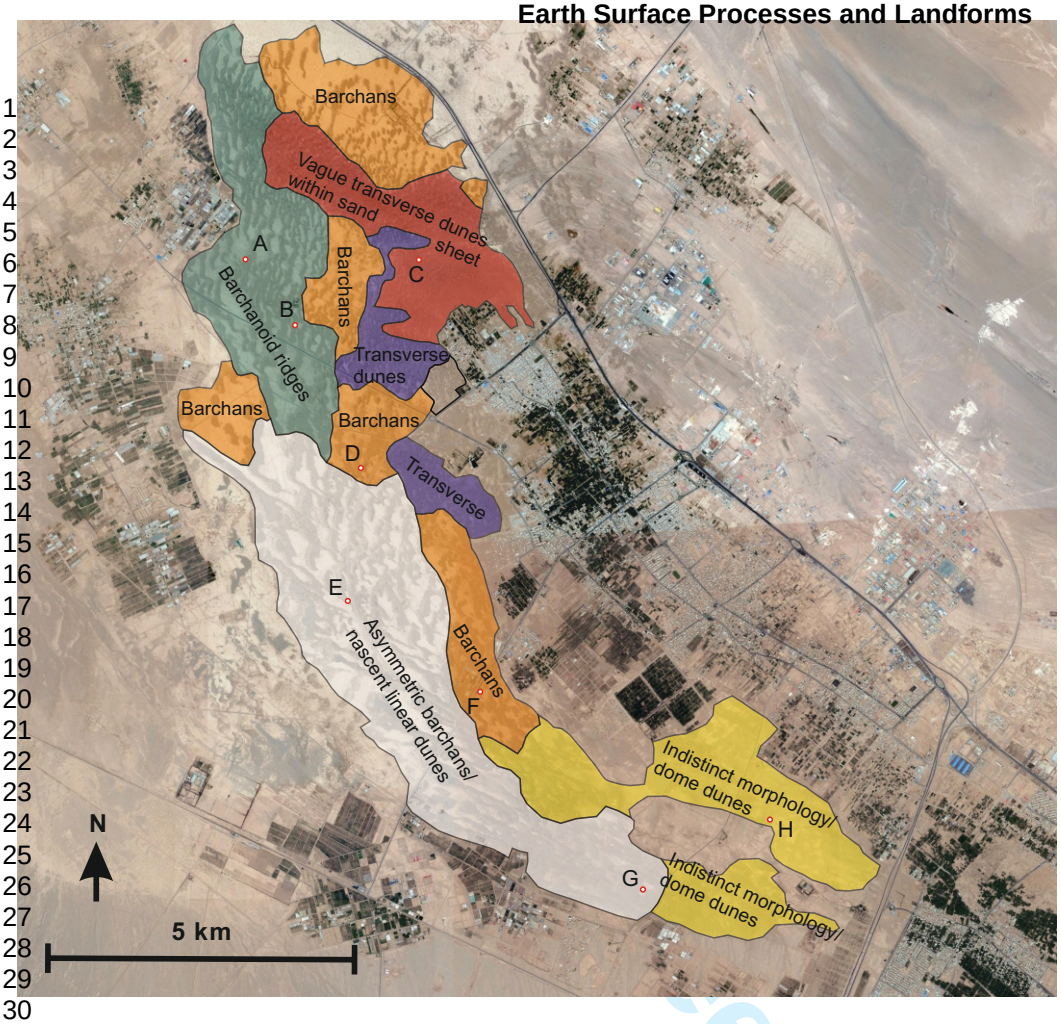

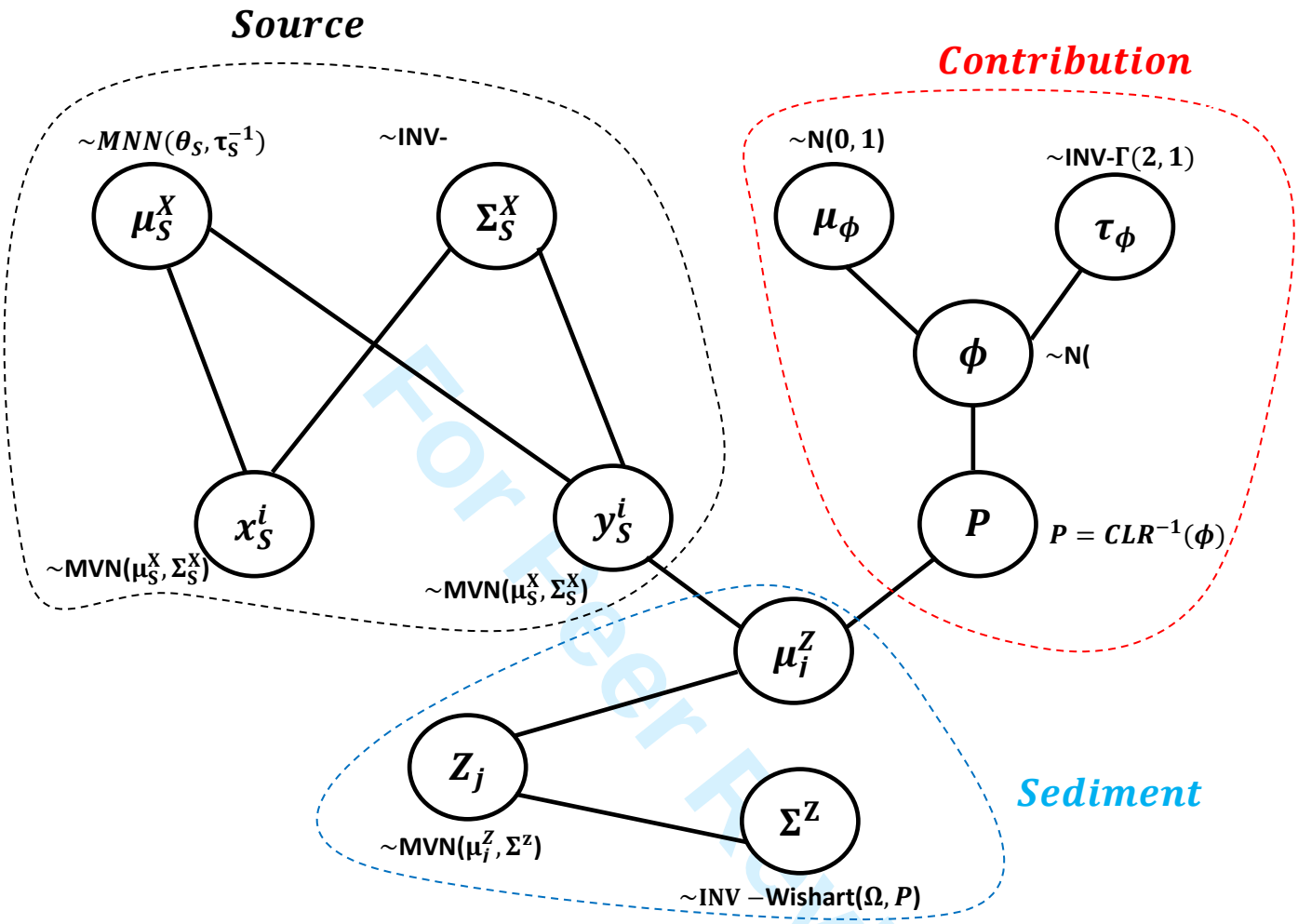

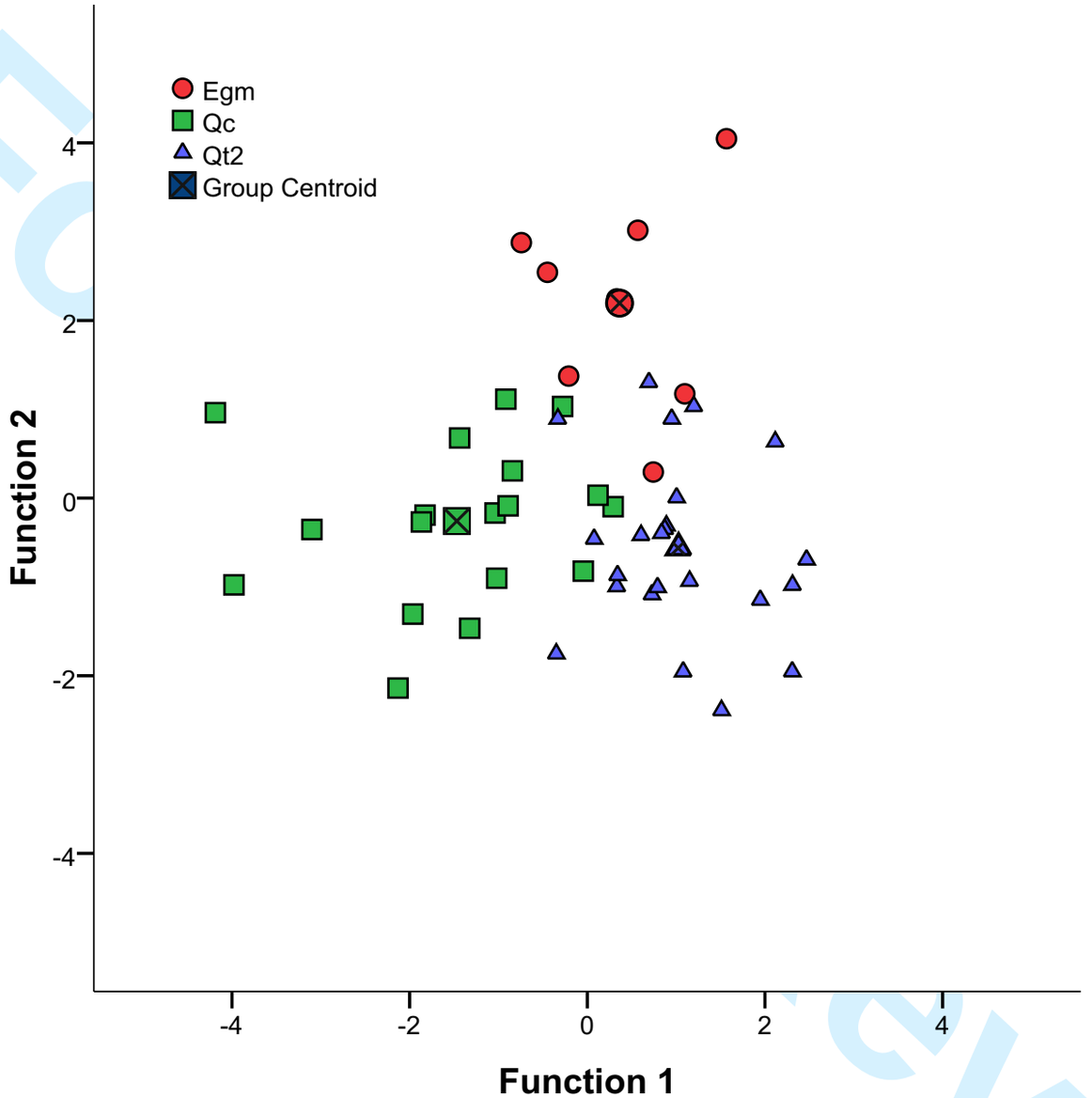

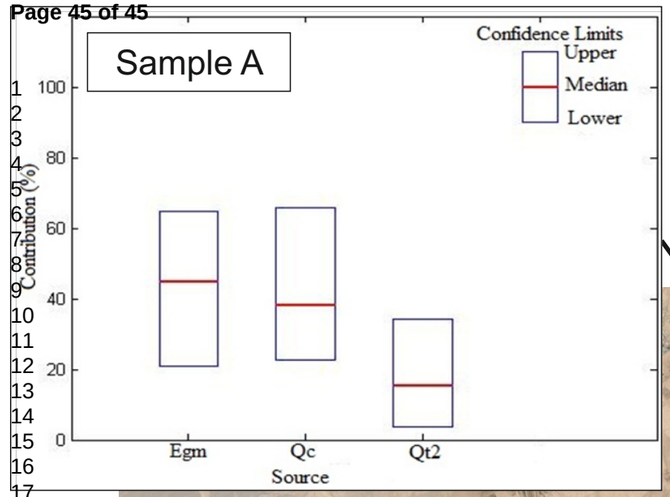
Sample A
Confidence Limits
Upper
Median
Lower
Contribution (%)
Egm
Qc
Qt2
Source

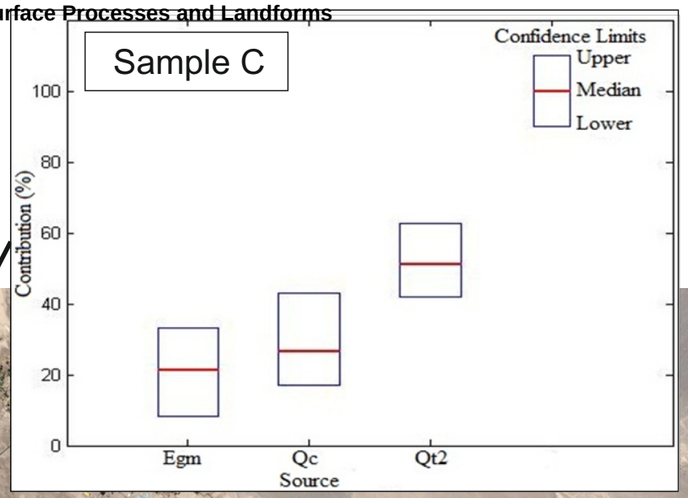
Sample C
Confidence Limits
Upper
Median
Lower
Contribution (%)
Egm
Qc
Qt2
Source

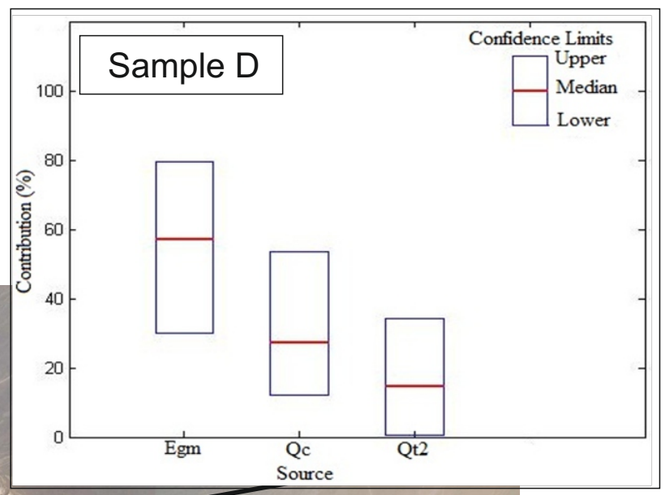
Sample D
Confidence Limits
Upper
Median
Lower
Contribution (%)
Egm
Qc
Qt2
Source

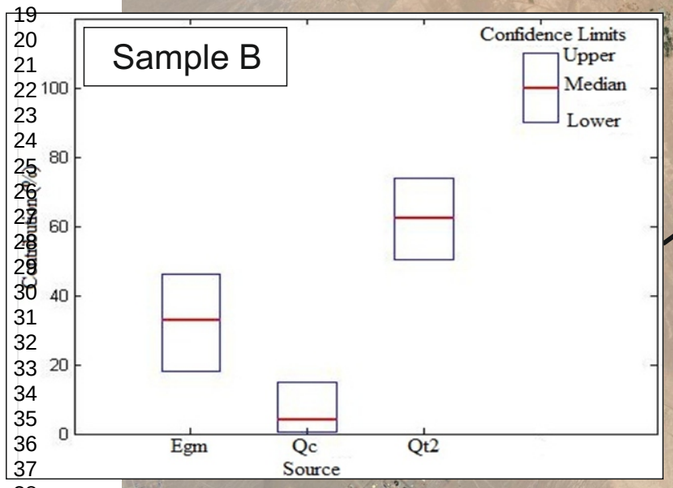
Sample B
Confidence Limits
Upper
Median
Lower
Egm
Qc
Qt2
Source

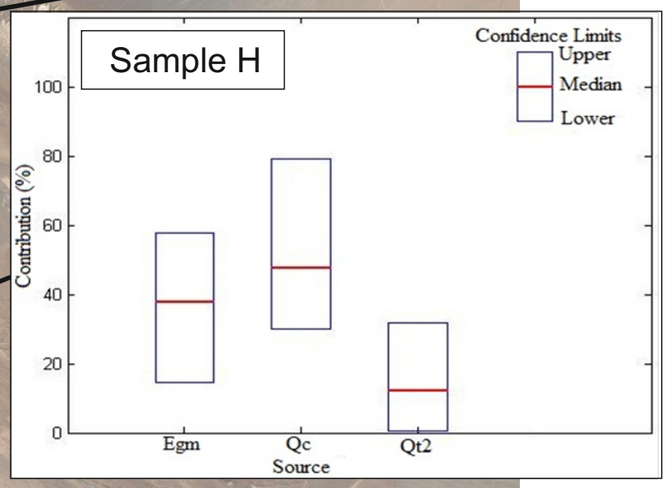
Sample H
Confidence Limits
Upper
Median
Lower
Contribution (%)
Egm
Qc
Qt2
Source

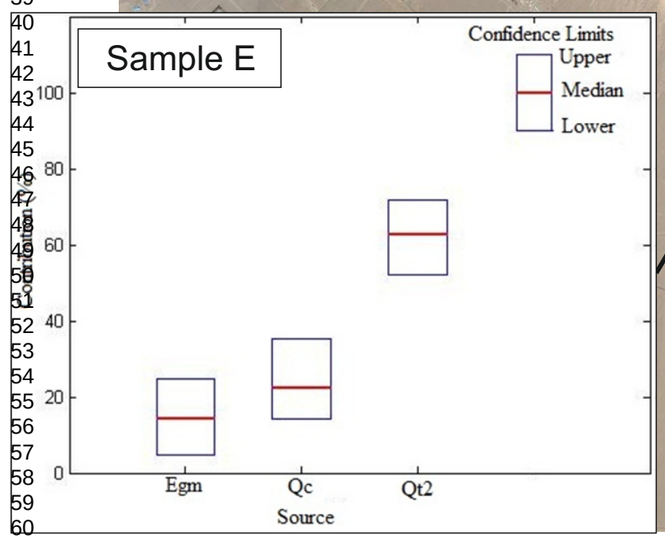
Sample E
Confidence Limits
Upper
Median
Lower
Egm
Qc
Qt2
Source

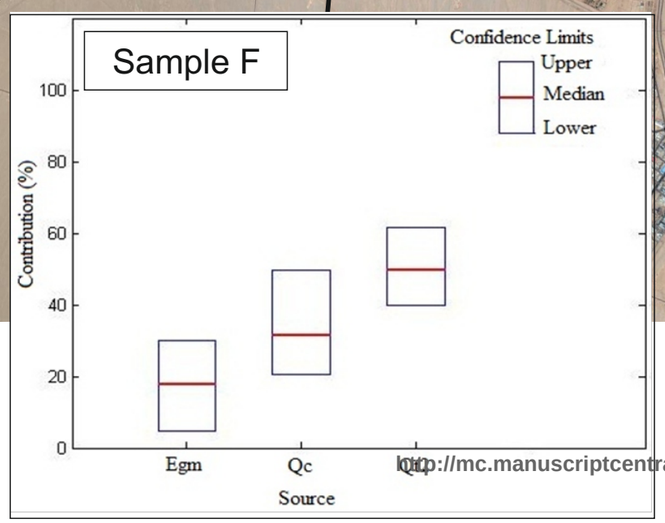
Sample F
Confidence Limits
Upper
Median
Lower
Contribution (%)
Egm
Qc
Qt2
Source

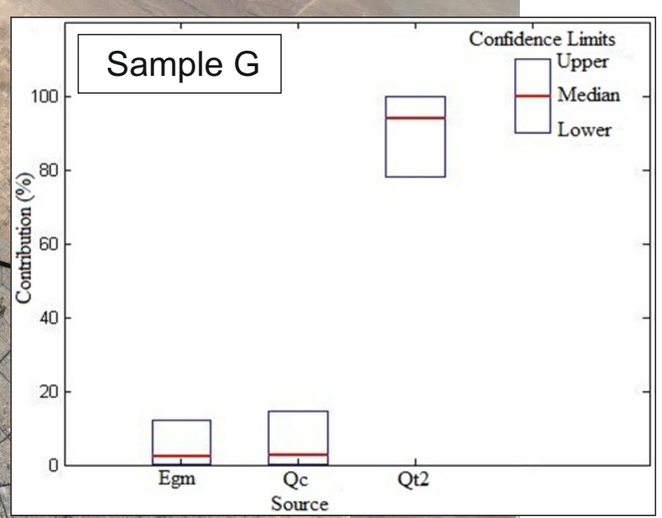
Sample G
Confidence Limits
Upper
Median
Lower
Contribution (%)
Egm
Qc
Qt2
Source

Ashkezar erg
N
5 km
Yazd